Eur. Phys. J. D **4**, 271–277 (1998)

THE EUROPEAN PHYSICAL JOURNAL D

Radiative electron capture into continuum in relativistic collisions of bare C ions with solid matter

G. Bednarz[1], A. Warczak[1,a], H. Tawara[2], T. Azuma[3], K. Komaki[3], and E. Takada[4]

[1] Jagiellonian University, Institute of Physics, Reymonta 4, Cracow 30-059, Poland
[2] National Institute for Fusion Science, Toki 509-5202, Japan
[3] College of Arts and Sciences, University of Tokyo, Komaba, Tokyo 153, Japan
[4] National Institute of Radiological Sciences, Anagawa, Chiba 263, Japan

Received: 3 May 1998 / Revised: 16 July 1998 / Accepted: 29 July 1998

Abstract. Continuum X-rays emitted from Be- and C-targets bombarded with 75–290 MeV/u C^{6+} ions were observed with an HPGe detector placed at 90° to the beam direction. In all spectra two components could be clearly distinguished: Radiative Electron Capture into Continuum (RECC) forming a characteristic edge, and Secondary Electron Bremsstrahlung (SEB) which dominates at high photon energies. The shape of the spectra was compared to a theoretical description. A special emphasis was given to the details of the RECC edge. It has been found that at the highest projectile energy of 290 MeV/u, in opposite to the lower beam energies, the detailed structure of this edge cannot be reproduced satisfactory within the approach applied.

PACS. 34. Atomic and molecular collision processes and interactions – 34.70.+e Charge transfer

1 Introduction

In collisions of fast heavy ions with light target atoms the projectile velocity is normally much larger than the orbital velocity of bound target electrons. Therefore, a target electron can be regarded as free and at rest in the laboratory. For such free electrons, capture into a charged projectile must be accompanied by the emission of a photon which carries away the energy and the momentum difference between the initial and final electron states. The photon spectra produced in these collisions, apart from characteristic target and projectile lines, consist of X-rays originating from the direct transfer of target electrons into the moving ion. The target electron may be captured into a bound state (Radiative Electron Capture – REC) or into a positive continuum state (Radiative Electron Capture into Continuum – RECC) of the projectile with simultaneous emission of a photon (Fig. 1). REC spectra consist of discrete lines while RECC forms continuous spectra which extend, in the projectile frame, from zero up to the edge energy corresponding to the kinetic energy T_r ($T_r = (m_e/m_p)T_p$, T_p: projectile kinetic energy; m_e, m_p: electron and projectile rest mass, respectively) of a target electron with respect to the projectile.

The REC process has been observed for the first time in the early 70's [1] and in the recent years was a subject of an extensive study (see *e.g.* [2–9]). The REC photons strongly dominate the spectra in collisions of very heavy projectiles with light target atoms. In the case of light projectiles (low atomic number Z) the X-rays are emitted mostly due to RECC, the process also called Primary Bremsstrahlung (PB) [10], Quasi-Free Electron Bremsstrahlung (QFEB) [11], or Radiative Ionization (RI) [12]. Unfortunately, in these collision systems, the weak REC lines match the region of RECC edge.

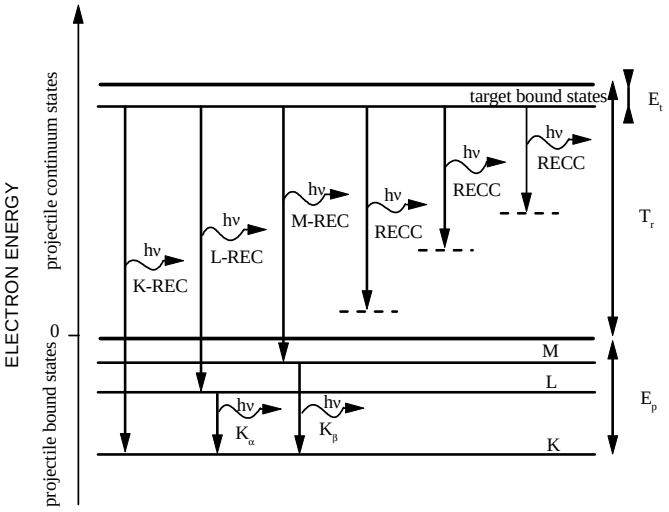

Fig. 1. Schematic presentation of REC and RECC processes, in the projectile frame. E_p, E_t are the electron binding energies in the projectile and target atoms, respectively.

[a] e-mail: ufwarcza@kinga.cyf-kr.edu.pl

The first RECC spectra were observed by Kienle *et al.* [13] and Schnopper *et al.* [14] followed by a study of the process in collisions of protons with low-Z targets [11,15,16] in the nonrelativistic velocity regime. Very recently, new ion-accelerator facilities (like SIS in Darmstadt or HIMAC in Chiba) opened an access to the relativistic collision regime where REC and RECC can be studied in detail [10,17–20].

Additionally, in solid targets secondary electrons, produced in primary projectile collisions with target atoms, generate a smooth continuum background due to bremsstrahlung (Secondary Electron Bremsstrahlung – SEB) [21,22]. The SEB spectrum is characterized by the high-energy limit at four times the RECC-edge energy ($4T_r$). The SEB energy limit is due to the maximum energy which can be transferred from the massive projectile to a free electron. In collisions of fast projectiles with thin targets the intensity of SEB X-rays is strongly reduced because of the escape of high-energy secondary electrons from the target.

In this work we present and analyze the results of the observation of RECC X-rays emitted in collisions of fast C^{6+} ions with solid matter (Be- and C- targets). For projectile energies (75–290 MeV/u), used in the experiment, the RECC spectrum extends up to 40–120 keV, respectively. For analysis we applied a nonrelativistic theoretical description of the process [11,23], based on the PWBA in the formulation adopted from Heitler [24], with relativistic and Coulomb deflection corrections added [15]. Moreover, the momentum distribution of target electrons and Doppler broadening of the spectra, arising from the observation geometry, were considered. A special fitting procedure [15] was applied to eliminate the background produced by secondary electrons (SEB). The shape of the remaining RECC spectra was analyzed in detail and emphasis was given mainly to the region close to the high energy limit. Here, the REC distribution was added, as well, in order to involve all possible processes contributing to the RECC edge in the case of low-Z projectiles.

2 Experiment

The measurements were performed at HIMAC (Heavy Ion Medical Accelerator in Chiba) at NIRS (National Institute of Radiological Sciences). HIMAC delivers low-Z ions up to Ar with energies up to 650 MeV/u, mainly for tumor therapy. However, a part of the beam time can be used directly for physics experiments.

In the present experiment (insert in Fig. 2a) C^{6+} ions were used which were preaccelerated by the linear accelerator, then stripped of their electrons and magnetically selected. The ions having well-defined charge state were directed to the main accelerator, which consists of two independent similar synchrotrons. Here, the final ion energies of 75, 150 and 290 MeV/u were reached.

Well-collimated ion beam bombarded 0.1 mm thick Be- and C-targets placed at 45° to the beam direction. The pulsed ion beam, with the repetition time of 2 or 3.3 s, was focused to a spot of 4 mm (75, 150 MeV/u) and 6 mm (290 MeV/u) in diameter. The averaged ion intensities, measured with a Faraday cup and an ionization chamber with an accuracy of about 30%, varied between 4×10^4 and 4.2×10^6 particles per second.

X-rays produced in collisions were detected in an ultrapure germanium detector (HPGe) (resolution of 650 eV FWHM at 122 keV) located outside the vacuum chamber 170 mm far away from the target at 90° to the beam direction. The observation window of the target chamber was made of a thin Mylar foil. The detector was equiped with a 19.3 mm thick Ge-crystal of 51.7 mm diameter separated by a 0.5 mm thick Be-window. In addition, an annular X-ray collimator with a diameter of 21 mm was inserted at a distance of 91.7 mm from the ion-bombarded target area. The collimator reduced the Doppler broadening of the observed X-rays. Finally, the X-ray detector covered the observation solid angle of $\Delta\Omega/4\pi = 3.3 \times 10^{-3}$. Single X-ray spectra were stored by a standard acquisition system. Energy calibration was performed using a ^{57}Co radioactive source.

In one of the runs, with 150 MeV/u ions bombarding a Be-target, an Al–Cu absorber (Al – 0.2 mm, Cu – 0.25 mm) was placed in front of the detector in order to enhance details of the RECC-edge structure.

Background spectra arising from ions passing through an empty target holder were registered in separate runs. The same ion energies and intensities, as in the runs with targets, were used.

3 Results and discussion

The experimental spectra were energy calibrated and corrected for detection efficiency (solid angle and absorption in Be-window of the detector). Absorption in the Mylar window of the target chamber was found to be negligible. Thereafter, using the number of collected projectiles and the absolute target thicknesses, the experimental double-differential cross-section values in the laboratory frame were obtained.

Figure 2 shows the spectra for all the three beam energies used. X-ray emission registered in collisions of C^{6+} ions with Be- and C-target is shown in Figures 2a and 2b, respectively. For all the combinations of target and beam energies two different spectra are displayed. The first one (top) is a raw spectrum and the second one (bottom) was obtained after subtraction of the normalized background produced by the beam in the target chamber (without target).

In all the spectra two continuous components are seen. Low-energy X-rays, produced mainly due to RECC, form a characteristic edge, enhanced in the background-corrected spectra. The high-energy limit of RECC X-rays (marked with arrows) was calculated for each projectile energy based on the energy conservation in kinematics. The position of RECC edge (38, 70, 121 keV) shifts with the projectile energy (75, 150, 290 MeV/u), respectively (see Fig. 2). The high-energy part of the spectra corresponds mainly to bremsstrahlung of the secondary

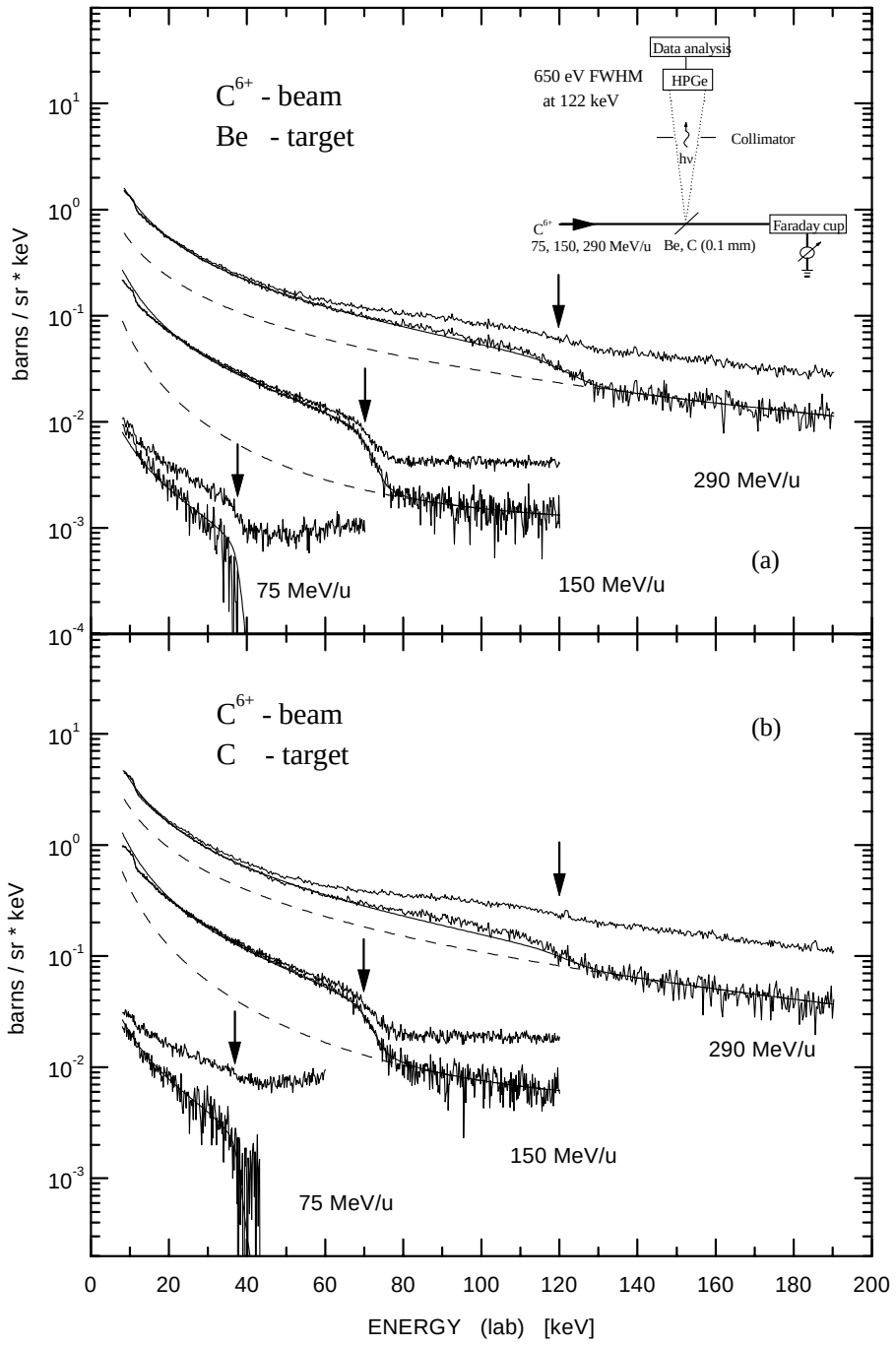

Fig. 2. Spectra observed in the experiment for: (a) Be-target, (b) C-target. For each energy-target combination two spectra are displayed. On the top – raw spectrum and lower – spectrum after background subtraction (for details see the text). For presentation purposes spectra were multiplied by factors; for Be-target: 1/20–75 MeV/u, 10–290 MeV/u; for C-target: 1/8–75 MeV/u, 10–150 MeV/u, 50–290 MeV/u. Dashed line: SEB contribution, solid line: RECC (relativistic approximation) + K-REC + SEB (for details see the text). Arrows show the RECC-edge energy T_r transformed to the laboratory frame. Insert in (a) represents the experimental setup.

electrons (SEB). In addition, in Figure 2, theoretical spectra, obtained as discussed below, are displayed.

For the analysis of the spectral shapes three radiative processes (RECC, K-REC and SEB) were taken into account. The experimental X-ray distribution in the laboratory, $F(\hbar\omega_L, k)$, was considered in the form:

$$F(\hbar\omega_L, k) = k\left(\frac{d^2\sigma^{REC}}{d\Omega_L d\hbar\omega_L} + \frac{d^2\sigma^{RECC}}{d\Omega_L d\hbar\omega_L}\right) + \frac{d^2\sigma^{SEB}}{d\Omega_L d\hbar\omega_L}, \quad (1)$$

where all the quantities have to be used in the laboratory frame; $\hbar\omega_L$ is photon energy, Ω_L denotes observation solid angle and $d^2\sigma^{REC}/d\Omega_L d\hbar\omega_L$, $d^2\sigma^{RECC}/d\Omega_L d\hbar\omega_L$, $d^2\sigma^{SEB}/d\Omega_L d\hbar\omega_L$ are theoretical double-differential cross-sections for REC, RECC and SEB, respectively, and k is a normalization coefficient determined from least-squares fit to the experimental data (background corrected).

First, using an approximate expression from [15], double-differential cross-sections in the laboratory frame for SEB ($d^2\sigma^{SEB}/d\Omega_L d\hbar\omega_L$ – dashed lines in Fig. 2) were obtained from the fits to the experimental spectra in the high X-ray energy region where RECC does not contribute

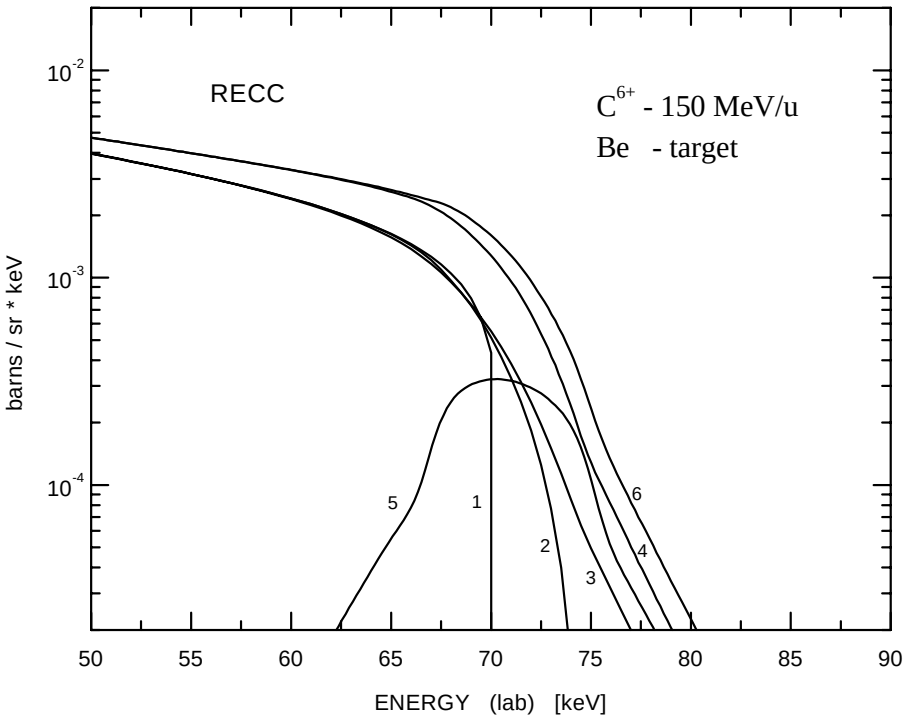

Fig. 3. Shape of the RECC spectrum calculated in the nonrelativistic approximation with relativistic corrections added: (1) for 90° observation angle; (2) averaged over the extended observation angle (83.5°–96.5°); (3) curve 2 corrected for the momentum distribution of target electrons (Compton profile); (4) curve 3 including the Elwert factor; (5) K-REC line averaged over the extended observation angle; (6) curve 4 with K-REC line added.

anymore:

$$\hbar\omega_L \frac{d^2\sigma^{SEB}}{d\Omega_L d\hbar\omega_L}(\hbar\omega_L, \theta_L) = \sum_{m=0} a_m(\theta_L)(\ln \hbar\omega_L)^m, \quad (2)$$

where θ_L is the observation angle in the laboratory frame and a_m denote fitting parameters. In accordance with [15] the best fits were achieved for $m = 2$.

Second, for the RECC process predictions of the nonrelativistic approach [11] corrected for relativistic effects according to [15] were applied for comparison with the experimental data. The expressions given for RECC cross-sections in the projectile frame were transformed to the laboratory and folded with the target-electron Compton profiles in free atoms [25].

In order to study details of the RECC edge, the impact of the observation geometry (insert in Fig. 2a) was also considered. The detector placed at the distance of 170 mm from the target covered, by considering the inserted X-ray collimator, approximately an angle of 13° (83.5°–96.5°) in the laboratory frame. Such a large observation angle distorts the shapes of registered X-ray spectra (Doppler broadening). Therefore, theoretical curves were averaged over all the angles covered by the detector and then compared to the experimental results.

Unfortunately, in our experiment, the charge state of the projectile after the collision was not registered, so that REC and RECC photons could not be separated. Therefore, as mentioned in the introduction, the REC photons contribute slightly to the RECC-edge region in the systems studied. In order to account for this small effect, the K-REC photon distribution, which dominates all REC transitions [8], was also added to the calculated spectra as anticipated by equation (1). Here, the nonrelativistic dipole approximation of Stobbe [26] in the form discussed in [8] was applied. The differential cross-sections for K-REC were folded with target-electron Compton profiles according to [8,23].

One has to point out that for our particular projectile-target combinations, at velocities investigated, the adiabaticity parameter η for REC process (comp. [8,17]) ranges approximately from about 70 up to 300. For these very high η values no experimental data on REC exist. So far, the exact relativistic treatment of REC [5,9] was tested experimentally only up to $\eta < 10$ [8]. In that η range the exact relativistic total cross-sections almost coincide with those of the nonrelativistic Stobbe formulation [8,17]. This equivalence does not hold for differential cross-sections. Here, however, strong discrepancies between nonrelativistic and relativistic formulation are found only at forward and backward observation angles [5,7] which are not relevant for our experiment.

Figure 3 shows, as an example, the influence of different correction factors on an ordinary RECC spectrum (curve 1) observed strictly at 90° and calculated in the nonrelativistic approximation including first order relativistic corrections (retardation effects) according to [15]. Curve 4, shown in Figure 3, involves all the corrections related to the detection geometry (extended solid angle), orbital motion of target electrons (Compton profiles), and the Coulomb deflection factor (Elwert factor [27,28]). Figure 3 is completed by curve 6 which includes the weak K-REC line, shown separately as curve 5.

All these corrections influence significantly the RECC-edge region only. Study of this particular spectrum region seems to provide a sensitive tool for testing RECC models and descriptions, provided other contributing factors are well controlled. It should be added that in the case

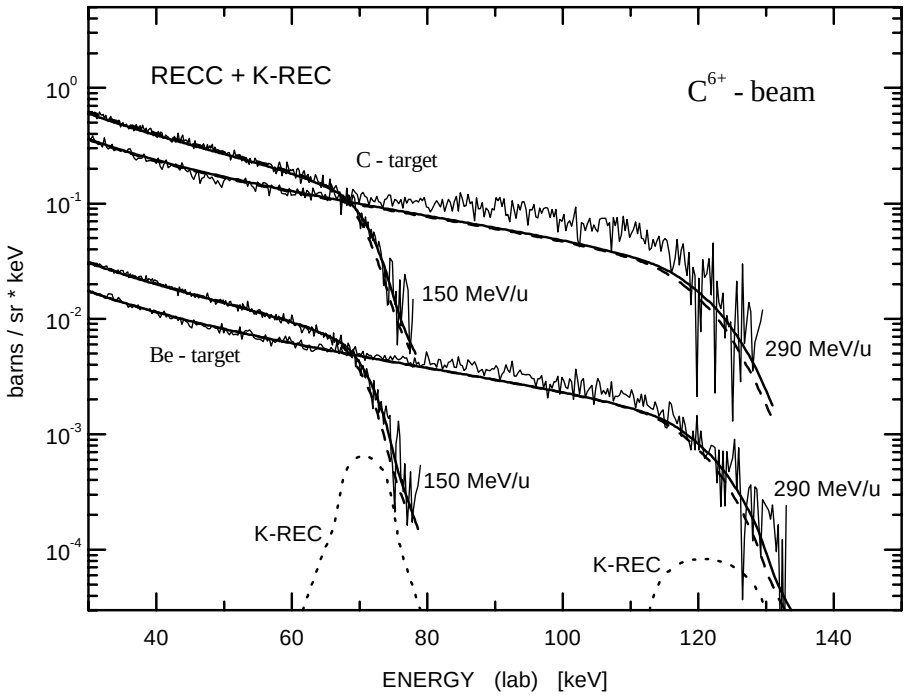

Fig. 4. Comparison between experimental data (background and SEB contribution subtracted) and theory (comp. Fig. 3). Dashed lines: RECC contribution (curve 4 from Fig. 3); dotted lines: K-REC (curve 5 from Fig. 3); solid lines: RECC and K-REC added. Cross-section values for C-target were multiplied by a factor of 50 for presentation purposes.

presented in Figure 3 the edge energy is shifted by as much as about 10 keV due to all the effects discussed.

In order to compare predictions of the discussed approximation (Fig. 3) with experimental results, the part of the spectra corresponding to SEB radiation (fitted according to Eq. (2)) was subtracted from the experimental data of Figure 2. Figure 4 shows the remaining spectra for 150 and 290 MeV/u ions and theoretical curves (curve 6 in Fig. 3) fitted to experimental data according to equation (1). The values of coefficient k obtained from the fitting procedure vary between 2.2 and 2.7. Similar results were obtained in [10,19]. A good agreement between the theoretical description and the experimental shape of the spectrum for 150 MeV/u ions is achieved. In the case of 290 MeV/u ions this agreement is not satisfactory. The experimental intensities of high-energy photons (70–120 keV) exceed theoretical predictions significantly (see Fig. 4).

The spectra described by the approximation applied, together with the SEB fits, are compared (full expression given by Eq. (1)), for completeness, with the background corrected experimental data in Figure 2 (solid line). In the case of 75 MeV/u ions the experimental statistics was not good enough to account properly for SEB. After background subtraction, RECC curves were fitted to the experimental spectra. Finally, for 75 and 150 MeV/u ions the shapes of X-ray spectra are very well reproduced by the theoretical description (Figs. 2, 4). For 290 MeV/u ions, in particular near RECC edge, the X-ray intensities are still stronger enhanced than predicted by a smooth theoretical curve. This discrepancy seems to be more pronounced for a C-target than for a Be-target (see Fig. 4). It turns out from the data presented in Figure 4 that, most probably, this discrepancy cannot be related to the REC process. A similar effect, of stronger than predicted high-energy radiation, was also observed [19] at GSI – Darmstadt for 223 MeV/u U^{90+} ions and gaseous targets (N_2, Ar, Kr, Xe) at various observation angles. The size of those discrepancies, close to the RECC-edge region, between theoretical and experimental cross-section values, seems to depend on the observation angle and at 90° amounts to a factor of about two, as in the present work.

During one of the experimental runs (150 MeV/u ions bombarding Be-target) an additional Al–Cu absorber was placed in front of the X-ray detector in order to expose the RECC-edge region. This region turns out to be very sensitive upon many experimental and theoretical factors, as already discussed. Therefore, the absorber thickness applied (see Sect. 2) was chosen to absorb strongly the intense low-energy radiation (below 40 keV) which can produce pile-up and distort the spectrum shape near the RECC edge. On the other hand the X-ray absorption in the RECC-edge region should be as low as possible in order to ensure an optimal detection efficiency. Figure 5 shows the experimental results corrected for all the efficiency factors, as for the other measurements. Theoretical shapes of X-ray spectra, calculated in analogy to solid lines presented in Figure 2, were multiplied by the corresponding absorption coefficients of Al–Cu absorber and then fitted to the experimental data (solid line in Fig. 5). An excellent agreement between experiment and theoretical description is obtained. In order to reveal all the details of the RECC-edge region, the SEB contribution (short-dashed line) was subtracted from the experimental data. The result of this procedure (dots in Fig. 5) represents solely the RECC-edge region and is compared, once more, with theoretical predictions (long-dashed line). For this particular collision system ($C^{6+} \rightarrow$Be) at 150 MeV/u

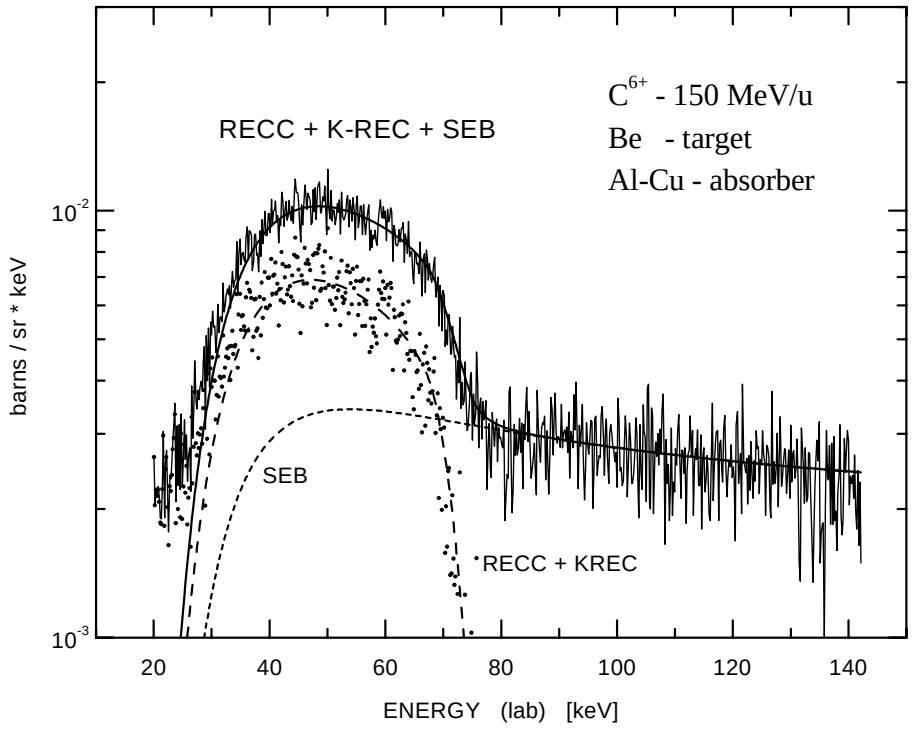

Fig. 5. Spectrum obtained with an Al–Cu absorber for Be-target and 150 MeV/u ions (back-ground subtracted). Dots: experimental data after SEB subtraction, solid line: RECC + K-REC + SEB contributions fitted according to equation (1), long-dashed line: RECC + K-REC contributions fitted to the dotted data, short-dashed line: SEB spectrum. All the theoretical lines (relativistic approximation) were corrected for the momentum distribution of the target electrons, for the broadening due to the observation angle and for the absorption in the Al–Cu absorber.

the result obtained in Figure 5 is consistent with that of Figure 2. It points to a negligible role of pile-up effect and supports the conclusion that the discrepancy observed for 290 MeV/u is probably due to the failure of the theoretical approximation applied.

4 Summary

For the analysis of experimental data presented, three radiative processes (RECC, SEB and K-REC) were considered. RECC, the main process contributing to the spectra in the investigated collision systems, was analyzed within a nonrelativistic approximation improved by adding relativistic corrections and the Coulomb deflection factor. In addition, corrections due to Compton profiles of target electrons and due to broadening caused by the large observation angle (Doppler broadening) were involved. The approach applied is in good agreement with the experimental data, especially for 75 and 150 MeV/u projectiles, where details of the shape of the RECC spectra were reproduced very nicely. However, distinct discrepancies between experiment and theory were observed for 290 MeV/u ions in the RECC-edge region. In all the cases the overall experimental X-ray intensities are larger than the theoretical predictions by a factor of about two which is consistent with other observations reported in the literature. This shows clearly that a more advanced theoretical description is required in order to account for all the discrepancies observed.

We have shown that the RECC-edge region is very sensitive to the details of the theoretical models applied. In particular, the corrections mentioned above (Compton profiles, Doppler broadening) shift the RECC edge to higher energies making it less steep. In addition, for the investigated light collision systems, the weak K-REC contribution is located on the RECC edge and cannot be easily separated from transitions into continuum states.

One has to stress that in the RECC-edge energy domain the final kinetic energy of the captured electron is very small as compared to the electron-nucleus interaction. Therefore, in this particular region one can probe the failure of the generally applied Born-approximation. This makes the discussed spectrum region very attractive for extended investigations where all the details should be treated with an extreme care, both theoretically and experimentally, in order to account for the discrepancies reported.

Further experiments looking very precisely onto RECC-edge region are planned in order to reveal the detailed mechanisms responsible for radiative capture processes in fast ion-atom collisions.

Support of one of the authors (A.W.) by a research project P014 at NIRS – HIMAC is gratefully acknowledged. A part of this work by G.B. and A.W. was supported by Polish Committee for Scientific Research (KBN) within grant No. 2P03B10910.

References

1. H.W. Schnopper, H.-D. Betz, J.P. Delvaille, K. Kalata, A.R. Sohval, K.W. Jones, H.E. Wegner, Phys. Lett. **29**, 898 (1972).
2. E. Spindler, H.-D. Betz, F. Bell, Phys. Rev. Lett. **42**, 832 (1979).

3. H. Tawara, P. Richard, K. Kawatsura, Phys. Rev. A **26**, 154 (1982).
4. W.E. Meyerhof, R. Anholt, J. Eichler, H. Gould, Ch. Munger, J. Alonso, P. Thieberger, H.E. Wegner, Phys. Rev. A **32**, 3291 (1985).
5. A. Ichihara, T. Shirai, J. Eichler, Phys. Rev. A **49**, 1875 (1994).
6. C.R. Vane, S. Datz, P.F. Dittner, J. Giese, N.L. Jones, H.F. Krause, T.M. Rosseel, R.S. Peterson, Phys. Rev. A **49**, 1847 (1994).
7. Th. Stöhlker, H. Geissel, H. Irnich, T. Kandler, C. Kozhuharov, P.H. Mokler, G. Muenzenberg, F. Nickel, C. Scheidenberger, T. Suzuki, M. Kucharski, A. Warczak, P. Rymuza, Z. Stachura, A. Kriessbach, D. Dauvergne, J. Eichler, A. Ichihara, T. Shirai, Phys. Rev. Lett. **73**, 3520 (1994).
8. Th. Stöhlker, C. Kozhuharov, P.H. Mokler, A. Warczak, F. Bosch, H. Geissel, R. Moshammer, C. Scheidenberger, J. Eichler, A. Ichihara, T. Shirai, Z. Stachura, P. Rymuza, Phys. Rev. A **51**, 2098 (1995).
9. J. Eichler, A. Ichihara, T. Shirai, Phys. Rev. A **51**, 3027 (1995).
10. R. Anholt, Ch. Stoller, J.D. Molitoris, D.W. Spooner, E. Morenzoni, S.A. Andriamonje, W.E. Meyerhof, H. Bowman, J.S. Xu, Z.Z. Xu, J.O. Rasmussen, D.H.H. Hoffmann, Phys. Rev. A **33**, 2270 (1986).
11. A. Yamadera, K. Ishii, K. Sera, M. Sebata, S. Morita, Phys. Rev. A **23**, 24 (1981).
12. R. Anholt, T.K. Saylor, Phys. Lett. A **56**, 455 (1976).
13. P. Kienle, M. Kleber, B. Povh, R.M. Diamond, F.S. Stephens, E. Grosse, M.R. Maier, D. Proetel, Phys. Rev. Lett. **31**, 1099 (1973).
14. H.W. Schnopper, J.P. Delvaille, K. Kalata, A.R. Sohval, M. Abdulwahab, K.W. Jones, H.E. Wegner, Phys. Lett. A **47**, 61 (1974).
15. T.C. Chu, K. Ishii, A. Yamadera, M. Sebata, S. Morita, Phys. Rev. A **24**, 1720 (1981).
16. K. Ishii, K. Sera, H. Arai, S. Morita, K. Tokuda, Phys. Rev. A **27**, 2225 (1983).
17. J. Eichler, W.E. Meyerhof, *Relativisic Atomic Collisions* (Academic Press, New York, 1995).
18. Th. Stöhlker, P.H. Mokler, C. Kozhuharov, A. Warczak, Comments At. Mol. Phys. **33**, 271 (1997).
19. T. Ludziejewski, Th. Stöhlker, S. Keller, H. Beyer, F. Bosch, O. Brinzanescu, R.W. Dunford, B. Franzke, C. Kozhuharov, D. Liesen, A.E. Livingston, G. Menzel, J. Meier, P.H. Mokler, H. Reich, P. Rymuza, Z. Stachura, M. Steck, L. Stennar, P. Świat, A. Warczak, J. Phys. B (submitted).
20. H. Tawara, T. Azuma, T. Ito, K. Komaki, Y. Yamazaki, T. Matsuo, T. Tonuma, K. Shima, A. Kitagawa, E. Takada, Phys. Rev. A **55**, 808 (1997).
21. F. Folkmann, J. Borggreen, A. Kjeldgaard, Nucl. Instr. Meth. **119**, 117 (1974).
22. K. Ishii, S. Morita, H. Tawara, Phys. Rev. A **13**, 131 (1976).
23. M. Kleber, D.H. Jakubassa, Nucl. Phys. A **252**, 153 (1975).
24. W. Heitler, *The Quantum Theory of Radiation* (Clarendon, Oxford, England, 1954).
25. F. Biggs, L.B. Mendelsohn, J.B. Mann, At. Data Nucl. Data Tables **16**, 201 (1975).
26. M. Stobbe, Ann. Phys. **7**, 661 (1930).
27. G. Elwert, Ann. Phys. **34**, 178 (1939).
28. G. Elwert, E. Haug, Phys. Rev. **183**, 90 (1969).